– For internal NASA and partners use only –

Lunar Impact Ejecta Model and Environment
A Brief Overview

Anthony M. DeStefano
NASA, MSFC, EV44

May 29, 2020

Contents

List of Figures

List of Tables

1 Executive Summary

2 Introduction

3 Input Environments

3.1 Sporadic Meteoroid Environment

3.1.1 Latitudinal Dependence of Primary Flux

3.1.2 Density Distribution Function

3.1.3 Mass Spectrum

3.2 Near-Earth Asteroid Environment

3.2.1 Speed Distribution

3.2.2 Mass Spectrum

4 Output Environment Format

4.1 Mass Limited Speed-Solid Angle Flux Distribution

5 Secondary Ejecta Model

5.1 Assumptions and Simplifications

There are several assumptions and simplications made in our model in order to provide traceable engineering solutions. We provide a list below with the most important assumptions in no particular order and provide comments on each.

1. The ejecta particle distribution is the same as the virgin regolith particle distribution.

    - Crater sizes that are less than ~ 50 m will mostly sample the top-most layer of regolith. For impactors that generate larger craters, such as those found in the NEA population, this assumption breaks down. We expect the very large craters (> 100 m) to introduce larger bolder sizes not present in the virgin regolith particle distribution. We believe these large bolders to be in the far tail of the distribution function and are very unlikely. Ignoring the large particle population will inflate the smaller particle sizes, which may help to offset the error in the risk, but this offset is not for certain.

2. The scaling law provided by *Housen and Holsapple* [2011] is valid for all impactors simulated in our model.

- Both authors are experts in the field of high-velocity impacts and have done much work to develop scaling laws that are valid for several orders of magnitude of impact sizes. For extremely small size impacts, such as impactor masses near 10^{-6} g, the scaling laws might not be valid since this is roughly the 50-percentile size of the regolith particle size distribution. For simplification, we ignore this issue for now.

3. The azimuth and zenith angle distribution functions are given empirically and do not depend on the size of impact or speed of impact, only the angle of impact.

    - The azimuth distribution function follows published work done by ESA contract work [*Miller*, 2017]. We modified the azimuth distribution function at highly oblique angles to include information about ejecta patterns that exhibit the so called butterfly patter [*Shuvalov*, 2011]. Depending on the latitude of the impact location, there can be a substantial component of the flux that can come into play.
    - The zenith angle distribution does have an azimuthal and impact angle dependence that follows fits from *Gault and Wedekind* [1978]. When the outgoing zenith angle tips over (when it goes negative), we ignore this component as an exclusion zone and implicitly include the fluxes in the downstream direction. This avoids having to deal with multi-valued functions which would require special cases to handle.
    - Since the integration is complicated enough, we do not want to complicate things by introducing a velocity dependence in the angle distributions. We know this to be the case in reality, but we ignore this dependence for simplicity.

4. The regolith density is constant over the whole Moon and for all depths.

    - The regolith density differs from highlands to mare in addition to depth. However, building a density map of the Moon is beyond the scope of this engineering model. We also note that the density dependence is raised to a small power (~ 0.2), so this will have a minor effect on total mass ejected from the crater. On the other hand, density can have a great impact on ballistic equations and bumper computations.

5. The Moon is a perfect sphere with a mono-polar gravity well (i.e., we ignore irregularities in the lunar surface and gravity).

    - We expect landing locations to not be deep in craters, which can be hazardous to con-ops. Local terrain can have a shadowing effect, so our calculations could be seen as a worst-case in this sense.
    - Most of the ejecta will have relatively short transit times and therefore will only be slightly perturbed by the irregular gravity well of the Moon. We also ignore Coriolis forces, which can be shown to be insignificant on the Moon for all relevant ejecta speeds.

5.2 Conversion from Primary to Secondary Flux

The total mass flux of secondary ejecta can be found from properties of the primary impactor. From *Housen and Holsapple* [2011], we can compute the mass ejected faster than v in terms of impactor properties, given by

$$M(v;\rho;m,\delta,U,\alpha) = M(>v) = C_4 m \left[\frac{v}{U\Theta(\alpha)}\left(\frac{\rho}{\delta}\right)^{\frac{3\nu-1}{3\mu}}\right]^{-3\mu}, \tag{1}$$

where

- v: secondary ejecta speed,
- ρ: target density,
- m: projectile mass,
- δ: projectile density,
- U: projectile speed,
- α: projectile impact angle (from horizon),

and

$$C_4 = \frac{3k}{4\pi} C_1^{3\mu}, \tag{2}$$

where the constants k, C_1, ν, and μ depend on the specific material properties, see Table 3 of *Housen and Holsapple* [2011]. The impact angle modification equation $\Theta(\alpha)$ can be chosen to be

$$\Theta(\alpha) = \begin{cases} 1 \\ \sin\alpha \\ \sin^\eta\alpha \end{cases}, \tag{3}$$

where typical values of η lie between 1 and 2. For the ejected mass that is in a given velocity range, we can define $\Delta M(v_2, v_1)$ as

$$\Delta M(v_2, v_1) = M(>v_2) - M(>v_1). \tag{4}$$

Equation (1) only gives us the total mass ejecta from the impact. We need to know what portion of that total mass reaches a particular region of interest. In essence, this is the major effort of the model outlined in this report. In the following section, we will show how to compute the portion of total mass.

5.3 Secondary Ejecta Distribution Function

The mass ejected from the crater, $M(>v)$, from Eq. (1), is the total mass ejected from an impact at velocities greater than v. However, we would like to know how this ejecta is distributed in speed and solid angle so we can map the ejecta to a particular surface location on the Moon. We can then set Eq. (1) in terms of the integral over the distribution functions of speed and solid angle as

$$M(>v) = \int_v^\infty \int_0^{2\pi} \int_0^{\pi/2} \sin\alpha d\alpha d\beta dv' F(\alpha) G(\beta) H(v'), \tag{5}$$

where α is the zenith angle, β is the azimuth angle, and v is the ejecta speed. Just to note, at the secondary impact location, the zenith angle will be the same as the ejected zenith angle. However, the azimuth angle (or bearing) will be modified due to travel across a spherical surface, see Section 5.7.

5.3.1 Speed Distribution Function

The speed distribution $H(v')$ is defined by

$$\int_v^\infty dv' H(v') = v^{-3\mu}, \tag{6}$$

which is the speed dependent term of Eq. (1). We can then solve the speed distribution explicitly as

$$H(v) = 3\mu v^{-(3\mu+1)}. \tag{7}$$

To integrate over the velocity distribution, we must take the results from Section 5.3.2 on the zenith distribution function and combine them with the above integral, giving

$$\begin{aligned}
&3\mu \int_{v_0}^{v_1} dv v^{-(3\mu+1)} \Delta x(v) \left[1 - \frac{x_0(v)+x_1(v)}{2}\right]^a \left[\frac{x_0(v)+x_1(v)}{2}\right]^{1/a} && (8)\\
=&3\mu \int_{v_0}^{v_1} dv v^{-(3\mu+1)} (\Delta m v + \Delta b)(1 - m_{avg} v - b_{avg})^a (m_{avg} v + b_{avg})^{1/a} && (9)\\
=&\int_{v_0}^{v_1} dv H_2(v), && (10)
\end{aligned}$$

where

$$\Delta m = m_1 - m_0, \tag{11}$$

$$\Delta b = b_1 - b_0, \tag{12}$$

$$m_{avg} = \frac{m_0 + m_1}{2}, \tag{13}$$

$$b_{avg} = \frac{b_0 + b_1}{2}. \tag{14}$$

This integral is related to the Appell F1 multivariate hypergeometric function and cannot be simplified to a finite number of single variable hypergeometric functions for generalized values of the exponent a. At this time, we will defer to integrate this equation numerically, preferably using the Romberg integration method.

Alternatively, we can attempt to generate an approximation. Taking the Taylor expansion of Equation (10) about v_{avg} out to the first term, we have (note, the first term drops out of the integral during integration, so the error is of order Δv^3)

$$\int_{v_0}^{v_1} dv H_2(v) \sim \int_{v_0}^{v_1} dv[H_2(v_{avg}) + H_2'(v_{avg})(v - v_{avg}) + \ldots], \tag{15}$$
$$= \Delta v H_2(v_{avg}),$$

$$= 3\mu\Delta v v_{avg}^{-(3\mu+1)}(\Delta m v_{avg} + \Delta b)(1 - m_{avg}v_{avg} - b_{avg})^a(m_{avg}v_{avg} + b_{avg})^{1/a}, \tag{16}$$

where

$$\Delta v = v_1 - v_0, \tag{17}$$

$$v_{avg} = \frac{v_0 + v_1}{2}. \tag{18}$$

5.3.2 Zenith Angle Distribution Function

To complete the integral over the zenith distribution, namely

$$\int_{\alpha_0(v)}^{\alpha_1(v)} d\alpha \sin\alpha F(\alpha), \tag{19}$$

we need to choose a distribution function for $F(\alpha)$ to allow for analytic solutions. We will therefore look for an alternate distribution given by the form

$$F(\alpha) = (1 - \cos\alpha)^{1/a}\cos^a\alpha, \tag{20}$$

where the exponent a can be defined in terms of the peak angle α_{max} as

$$a = \frac{\cos\alpha_{max}}{1 - \cos\alpha_{max}} = \frac{\cos\alpha_{max}}{2\sin^2(\alpha_{max}/2)}, \tag{21}$$

such that $F'(\alpha_{max}) = 0$ and $F''(\alpha_{max}) < 0$.

In order to compare with experiments for the peak angle α_{max}, we can use Figure 18 of *Gault and Wedekind* [1978] as a proxy to our model of α_{max}, as a function of the azimuth angle. Using a third order polynomial for both fits to the downstream and upstream angles given in Table 1, we arrive at

$$\alpha_{max}(\beta - \beta_i = \pi) = 0.0003\alpha_i^3 - 0.036\alpha_i^2 + 1.5206\alpha_i + 20, \text{ downstream} \tag{22}$$

$$\alpha_{max}(\beta - \beta_i = 0) = -0.00042\alpha_i^3 + 0.0236\alpha_i^2 + 0.129\alpha_i + 20, \text{ upstream} \tag{23}$$

in units of degrees, where β_i is the impact azimuth angle, β is the ejecta azimuth angle, and α_i is the impact zenith angle. For other values of $\beta - \beta_i$, we can write a complete function as

$$\alpha_{max}(\beta) = \alpha_{max}(\beta - \beta_i = \pi)\cdot\sin^2\left(\frac{\beta - \beta_i}{2}\right) + \alpha_{max}(\beta - \beta_i = 0)\cdot\cos^2\left(\frac{\beta - \beta_i}{2}\right), \tag{24}$$

or rewriting we have

$$\alpha_{max}(\beta) = \frac{\alpha_{max,0} + \alpha_{max,\pi}}{2} - \frac{\alpha_{max,\pi} - \alpha_{max,0}}{2}\cos(\beta - \beta_i), \tag{25}$$

and solving for $\beta - \beta_i$, after setting $\alpha_{max}(\beta)$ to zero,

$$\arccos\left(\frac{\alpha_{max,0} + \alpha_{max,\pi}}{\alpha_{max,\pi} - \alpha_{max,0}}\right) = \beta - \beta_i. \tag{26}$$

As a simplification, we can approximate the $\cos(\beta - \beta_i)$ term as (note, this is not a Taylor series)

$$\cos(\beta - \beta_i) \sim 1 - \left|\frac{\beta - \beta_i}{\pi/2}\right|, \tag{27}$$

for $-\pi \leq \beta - \beta_i \leq \pi$ such that $\cos\alpha_{max}$ becomes

$$\cos\alpha_{max} \sim \cos\left[\alpha_{max,0} + \frac{\alpha_{max,\pi} - \alpha_{max,0}}{\pi}|\beta - \beta_i|\right] \tag{28}$$

Table 1: Cone angles of upstream and downstream of impact derived from Figure 18 of *Gault and Wedekind* [1978].

Impact Zenith Angle	Upstream Zenith Angle	Downstream Zenith Angle
0	20	20
15	24	35
30	35	45
45	28	40
60	13	54
75	-35	66

Using Table 1 as a fit for the peak angle α_{max} is an approximation since the tabular data is only for a specific snapshot of the ejecta at a side view, $90°$ from the impact direction. The zenith distribution should also be a function of the ejecta speed, but we do not make this assumption for the sake of simplicity. According to this model, starting around $60° - 70°$, there is a region of exclusion for a part of the zenith distribution upstream of the impact, see Figure 1.

Next, we can do a variable substitution (chosen so the domain of the zenith angle to the new variable goes from $\alpha \in [0, \pi/2]$ to $x \in [0, 1]$)

$$1 - x = \cos\alpha, \tag{29}$$
$$dx = \sin\alpha d\alpha, \tag{30}$$

so that Eq. (19) becomes

$$\int_{x_0(v)}^{x_1(v)} dx x^{1/a}(1-x)^a, \tag{31}$$

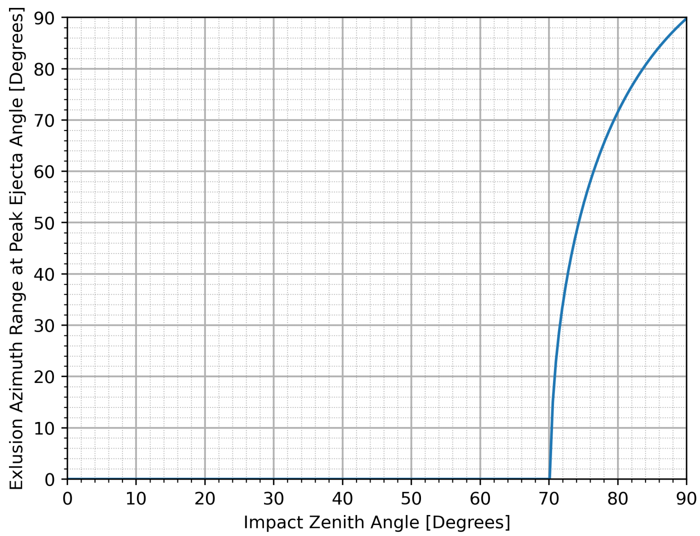

Figure 1: For larger impact angles that are more grazing to the surface, the zenith and azimuth ejecta distributions become asymmetric. Starting at $70°$, the peak ejecta angle α_{max} becomes negative in an exclusion range, as shown in the figure. This means that the $-\alpha_{max} \to \alpha_{max}$ and $\beta - \beta_i \to \beta - \beta_i + \pi$. In this model, for impact angles near $90°$, most of the ejecta is concentrated in the downstream direction.

where the equations $x_0(v)$ and $x_1(v)$ are a linear function of v and an implicit function of the distances D_0 and D_1, respectively. The integral in Eq. (31) is the incomplete beta function

$$\int_{x_0(v)}^{x_1(v)} dx x^{1/a}(1-x)^a = \beta(x_1(v); 1/a+1, a+1) - \beta(x_0(v); 1/a+1, a+1). \quad (32)$$

Note that the normalization term for $\alpha \in [0, \pi/2]$ is given by

$$\int_0^{\pi/2} d\alpha \sin\alpha F(\alpha) = \beta(1/a+1, a+1) = \frac{\Gamma(1/a+1)\Gamma(a+1)}{\Gamma(a+1/a+2)}, \quad (33)$$

which includes ejecta at speeds greater than the escape speed.

For small differences in D_0 and D_1, we can roughly assume small differences[1] in $x_0(v)$ and $x_1(v)$ so that we can write Eq. (32) in terms of a derivative, where we

[1] If Δx is not small, then we can partition the x range into smaller pieces so that Δx is small, which will be the case in almost all circumstances.

evaluate the derivative at the midpoint

$$
\begin{aligned}
&\beta(x_1(v); 1/a+1, a+1) - \beta(x_0(v); 1/a+1, a+1) \\
=&\frac{\beta(x_0(v)+\Delta x; 1/a+1, a+1) - \beta(x_0(v); 1/a+1, a+1)}{\Delta x}\Delta x \\
\approx&\Delta x \frac{d}{d(x_0(v))}\beta(x_0(v); 1/a+1, a+1)\Big|_{x_0(v)\to x_0(v)+\Delta x/2} \\
=&\Delta x\,[1-x_0(v)]^a\, x_0^{1/a}(v)\Big|_{x_0(v)\to x_0(v)+\Delta x/2} \\
=&\Delta x(v)\left[1-\frac{x_0(v)+x_1(v)}{2}\right]^a\left[\frac{x_0(v)+x_1(v)}{2}\right]^{1/a},
\end{aligned} \tag{34}
$$

where $\Delta x(v) = x_1(v) - x_0(v)$, and (note, the v's are normalized by v_{esc}, emitted for clarity)

$$x_0(v) = m_0 v + b_0, \tag{35}$$

$$x_1(v) = m_1 v + b_1, \tag{36}$$

$$\Delta x(v) = (m_1 - m_0)v + b_1 - b_0. \tag{37}$$

The coefficients m_0, m_1 and b_0, b_1 are implicit functions of the distances D_0, D_1. For the $j-$th distance D_j and the $i-$th speed v_i, the m and b coefficients can be written as

$$m_{j,i}^{\pm} = \frac{v_{i+1} - v_i}{x_{j,i+1}^{\pm} - x_{j,i}^{\pm}}, \tag{38}$$

$$b_{j,i}^{\pm} = v_i - m_{j,i}^{\pm}\cdot x_{j,i}^{\pm}, \tag{39}$$

where

$$x_{j,i}^{\pm} = 1 - \cos\alpha_{j,i}^{\pm}, \tag{40}$$

for

$$\cos^2\alpha_{j,i}^{\pm} = \frac{v_i^2 + \tan^2\left(\frac{D_j}{2r_m}\right)(2v_i^2-1) \pm \sqrt{v_i^4 + \tan^2\left(\frac{D_j}{2r_m}\right)(2v_i^2-1)}}{2v_i^2\left(1+\tan^2\left(\frac{D_j}{2r_m}\right)\right)}, \tag{41}$$

taking the positive root, $\cos\alpha_{j,i}^{\pm} = +\sqrt{\cos^2\alpha_{j,i}^{\pm}}$, since $\alpha \in [0, \pi/2]$. Other useful transformed equations are

$$\tan\left(\frac{D_j}{2r_m}\right) = \frac{2v_i^2(1-x_{j,i}^{\pm})\sqrt{x_{j,i}^{\pm}(2-x_{j,i}^{\pm})}}{1-2v_i^2 x_{j,i}^{\pm}(2-x_{j,i}^{\pm})}, \tag{42}$$

from Eq. (68), and

$$v_i = \frac{1}{\sqrt{2(1-x_{j,i}^{\pm})\sqrt{x_{j,i}^{\pm}(2-x_{j,i}^{\pm})}\cot\left(\frac{D_j}{2r_m}\right) + 2x_{j,i}^{\pm}(2-x_{j,i}^{\pm})}}, \tag{43}$$

from Eq. (71). Solving for $x^{\pm}_{j,i}$ in either equation, we can now write x explicitly in terms of the distance D and ejecta speed v as

$$x^{\pm}_{j,i} = 1 - \sqrt{\frac{v_i^2 + \tan^2\left(\frac{D_j}{2r_m}\right)(2v_i^2 - 1) \pm \sqrt{v_i^4 + \tan^2\left(\frac{D_j}{2r_m}\right)(2v_i^2 - 1)}}{2v_i^2\left[1 + \tan^2\left(\frac{D_j}{2r_m}\right)\right]}}. \tag{44}$$

For a given distance, the domain of x is given by (for v up to 1)

$$x^{\pm}_{j,i} \in \left(1 - \cos\left(\frac{D_j}{4r_m}\right), 1\right), \tag{45}$$

and the domain of v is given by

$$v_i \in \begin{cases} \left(\left[1 + \left|\cos\left(\frac{D_j}{2r_m}\right)\right| \cot\left(\frac{D_j}{2r_m}\right) + \sin\left(\frac{D_j}{2r_m}\right)\right]^{-1/2}, 1\right) & \text{for } D_j < \pi r_m \\ \left(\frac{\sqrt{2}}{2}, 1\right) & \text{for } D_j \geq \pi r_m \end{cases} \tag{46}$$

where the value of $x^{\pm}_{j,i}$ at the minimum of v_i is

$$x^{\pm}_{j,i} = 1 - \sqrt{\frac{1 - \sin\left(\frac{D_j}{2r_m}\right)}{2}} \tag{47}$$

The two domains in Eqs. (45) and (46) define the region of interest, and allow for the integration to begin at the correct outermost boundary lines.

There are three regions of the zenith angle-space, and hence the x-space, where we have:

Region I: For all valid distances D_j and D_{j+1}, use $m^+_{j,i}$, $b^+_{j,i}$, $m^+_{j+1,i}$ and $b^+_{j+1,i}$

Region II: For $D_j < \pi r_m$ and all D_{j+1}, use $m^-_{j,i}$, $b^-_{j,i}$, $m^+_{j+1,i}$ and $b^+_{j+1,i}$

Region III: For $D_j < \pi r_m$ and $D_{j+1} < \pi r_m$, use $m^-_{j,i}$, $b^-_{j,i}$, $m^-_{j+1,i}$ and $b^-_{j+1,i}$

5.3.3 Azimuth Angle Distribution Function

The azimuth distribution shown below is given by [*Rival and Mandeville*, 1999]

$$G(\beta) = \begin{cases} \frac{1}{2\pi}\left[\frac{3\alpha_i}{2\pi - 3\alpha_i}\cos(\beta - \beta_i) + 1\right] & \text{for } \alpha_i \leq \pi/3 = 60^\circ \\ \frac{1}{\sigma'\sqrt{2\pi}}\exp\left[-\frac{(\beta - \beta_i)^2}{2\sigma'^2}\right] & \text{for } \alpha_i > \pi/3 = 60^\circ \end{cases}, \tag{48}$$

where

$$\sigma' = \frac{\pi}{36} = 5^\circ, \tag{49}$$

for β_i the impact azimuth angle + π.

Alternative Azimuth Distribution: The piece-wise function defined in Equation (48) for the azimuth distribution is correctly normalized for impact zenith angles $\alpha_i \leq 60°$, however for angles greater than $60°$, the function is not continuous across the boundary $\beta = 2\pi \to 0$. We would also like a continuous function across the piece-wise boundary as well.

Our proposed azimuth distribution is as follow. We will use the $\alpha_i \leq 60°$ functional form in Equation (48), but we will have a different large-angle expression. The new azimuth distribution is defined as

$$G(\beta) = \begin{cases} \frac{1}{2\pi}\left[\frac{3\alpha_i}{2\pi-3\alpha_i}\cos(\beta-\beta_i)+1\right] \text{ for } \alpha_i \leq \pi/3 = 60° \\ \frac{1}{A}\left[\exp\left[-\frac{(\beta-\beta_i-2(\alpha_i-\alpha_{i,0}))}{\pi b}\right] + \exp\left[-\frac{(\beta-\beta_i+2(\alpha_i-\alpha_{i,0}))}{\pi b}\right]\right] \text{ for } \alpha_i > \pi/3 \end{cases}, \tag{50}$$

where

$$b = \frac{0.05-1}{\pi/2-\pi/3}(\alpha_i-\alpha_{i,0})+1 = \frac{3}{10\pi}(\alpha_i-\alpha_{i,0})+1, \tag{51}$$

and

$$\alpha_{i,0} = \pi/3. \tag{52}$$

For the second case, we empirically include information about the *butterfly pattern* that is seen for highly oblique impact angles [e.g., *Shuvalov*, 2011]. The size of the impactor will affect the spread of the butterfly pattern, but we assume a certain spread profile for all impactor sizes.

The normalization[2] constant for the $\alpha_i > \pi/3$ case is

$$A = \sqrt{b}\pi\left[\text{erf}\left(\frac{\pi+2(\alpha_i-\alpha_{i,0})}{\sqrt{\pi b}}\right) + \text{erf}\left(\frac{\pi-2(\alpha_i-\alpha_{i,0})}{\sqrt{\pi b}}\right)\right], \tag{53}$$

when integrating $\beta - \beta_i$ from $-\pi$ to π. However, when integrating the outgoing secondary azimuth angle β with respect to the impact azimuth angle β_i when there is an exclusion zone defined by $\pm\Delta\beta_{ez}$, the normalization constant is

$$A = \sqrt{b}\pi\left[\text{erf}\left(\frac{\pi-\Delta\beta_{ez}+2(\alpha_i-\alpha_{i,0})}{\sqrt{\pi b}}\right) + \text{erf}\left(\frac{\pi-\Delta\beta_{ez}-2(\alpha_i-\alpha_{i,0})}{\sqrt{\pi b}}\right)\right], \tag{54}$$

which is appropriate for any $\alpha_i > \pi/3$ for an exclusion zone $\Delta\beta_{ez}$ given by (using Eq. (28) = $\pi/2$)

$$\Delta\beta_{ez} = \begin{cases} \pi\frac{-\alpha_{max,\pi}}{\alpha_{max,0}-\alpha_{max,\pi}}, \text{ for } \alpha_{max,\pi} < 0 \\ 0, \text{ otherwise} \end{cases} \tag{55}$$

For $\alpha_i > \pi/3 = 60°$, in order to integrate over a small azimuth range $\beta \in (\beta_0, \beta_1)$

[2] Please note that this is not the exact normalization. This is assuming that the altitude distribution does not depend on the azimuth, which is not the case. We only include this here to *help* the overall normalization once we calculate it, which will have to be done by a numerical integral.

For $\alpha_i \leq \pi/3 = 60°$, integrating over a small range $\Delta\beta = \beta_1 - \beta_0$, the integral is given by

$$\begin{aligned} &\frac{1}{2\pi}\int_{\beta_0}^{\beta_1} d\beta \left[\frac{3\alpha_i}{2\pi - 3\alpha_i}\cos(\beta - \beta_i) + 1\right] \\ =&\frac{1}{2\pi}\left[\Delta\beta + \frac{3\alpha_i}{2\pi - 3\alpha_i}\left[\sin(\beta_1 - \beta_i) - \sin(\beta_0 - \beta_i)\right]\right]. \end{aligned} \tag{56}$$

5.4 Lunar Regolith Properties

All of the lunar regolith properties are derived from tables that were generated in Section 3.4.2 of SLS-SPEC-159 (DSNE). Specifically, Table 3.4.2.3-1 contains a summary of the bulk regolith properties. Note that a specific gravity of 3.1 is synonymous to a density of 3100 kg m^{-3}, which is used in our model as the average regolith particle density. We assume the regolith density to be the same all over the lunar surface.

For the scaling law given in Equation (1), we model the regolith as sand fly ash [*Housen and Holsapple*, 2011] since a porosity of 45 matches the closest to DSNE Table 3.4.2.3-1.

5.5 Secondary Particle Size Distribution Function

For relatively small impact sizes (craters $< 30 - 50$ m), we can generally assume the secondary ejecta follows that of the original regolith. The cumulative distribution function (CDF) of the particle sizes can be fit to many observations, as shown in Figure 2.

In order to parameterize the CDF from Figure 2, we make a fit to the model equation

$$C_{moon} = 1 - \exp\left(\frac{-1}{ax^b + cx^d}\right), \tag{57}$$

which is an exponential distribution with two scales defined by a and c, with x in units of mm. In SciDAVis, we make the fit with the x-axis on a logarithmic scale to give equal weight to both small and large scaled particles. The results for the curve fit are shown in Figure 3. We found that a simple exponential distribution with a single scale was insufficient, hence the reason we opted for a two-scaled exponential distribution.

To compute the probability distribution function (PDF), we can simply take the derivative of the CDF with respect to x, which results in the following equation:

$$P_{moon} = -A\frac{abx^{b-1} + cdx^{d-1}}{(ax^b + cx^d)^2}\exp\left(\frac{-1}{ax^b + cx^d}\right), \tag{58}$$

where A is the normalization constant. In theory, this should be equal to 1, but since we are not taking our particle size from 0 to infinity, we need to compute the value of A. If we assume the particle size can range from 0.001 mm to 10 mm, then $A = 1.02218$.

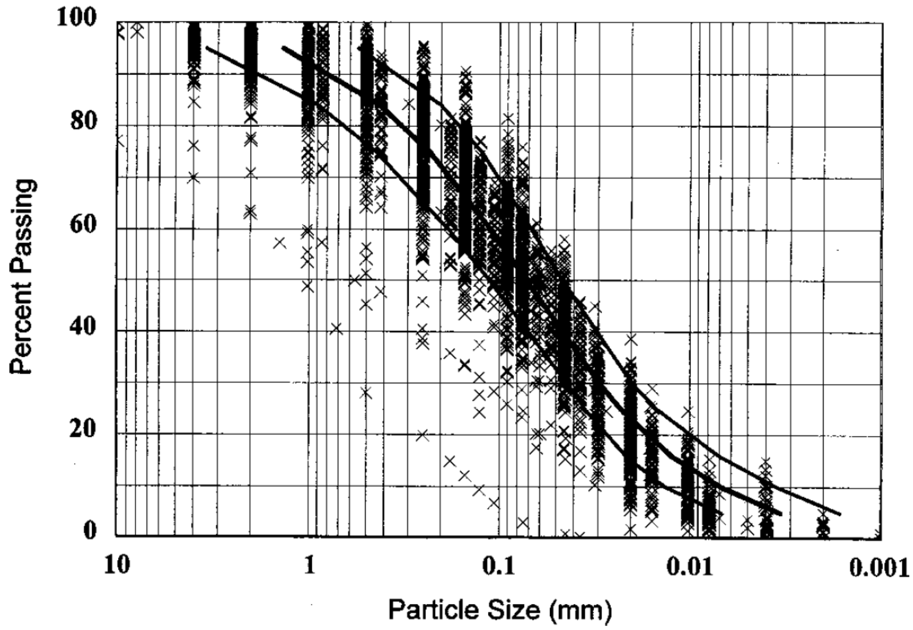

Figure 2: Geotechnical particle size distribution: middle curve showing the average distribution; left-hand and right-hand curves showing ± 1 standard deviation [*Carrier III*, 2003].

```
[12/30/2019 5:40:09 PM          Plot: "Graph2"]
Non-linear fit of dataset: Table2_2, using function: 100*(1-exp(-1/(a*(10^x)^b+c*(10^x)^d)))
Y standard errors: Unknown
Nelder-Mead Simplex algorithm with tolerance = 0.0001
From x = -2.482108151 to x = 0.134259956
a  = 0.0548044684398436 +/- 0.00569348851446585
b  = -1.01472478485333 +/- 0.0196858460040614
c  = 0.337499285612252 +/- 0.0049924392579481
d  = -0.251808155531636 +/- 0.0188844274561765
---------------------------------------------------------------------------------------
Chi^2 = 8.25978651917647
R^2 = 0.999849854428033
---------------------------------------------------------------------------------------
Iterations = 89
Status = success
---------------------------------------------------------------------------------------
```

Figure 3: Non-linear fit of Figure 2 (the average distribution) with Eq. 57 in SciDAVis, giving the constants for a, b, c, and d.

5.6 Ejecta Distance, Speed, and Angle Relations

We would like to relate the distance from the meteorite impact to the secondary ejecta impact site by the secondary ejecta speed v and angle γ from zenith. If we assume the Moon is a perfect sphere with no atmosphere, we can calculate this distance by following the elliptical path the ejecta makes. The semi-major axis and eccentricity of the elliptical orbit are given by[3]

$$\frac{a}{r_m} = \frac{1}{2\left(1 - \frac{v^2}{v_{esc}^2}\right)}, \tag{59}$$

where $r_m = 1737.1$ km is the radius of the Moon and $v_{esc} = 2.38$ km/s is the Moon's escape velocity, and

$$e = \sqrt{\left(\frac{2v^2}{v_{esc}^2} - 1\right)^2 \sin^2\gamma + \cos^2\gamma}, \tag{60}$$

where we employed the fact that the gravity of the Moon is $g = GM/r_m^2$ and the escape velocity is related by $v_{esc} = \sqrt{2gr_m}$. The third equation we need gives the location in the elliptical orbit by the angle β from the perilune, the semi-major axis a, and the eccentricity e by

$$r = \frac{a(1-e^2)}{1 + e\cos\beta}. \tag{61}$$

Solving for $\cos\beta$ in Eq. 61, we have

$$\cos\beta = \frac{1}{e}\left(\frac{a(1-e^2)}{r} - 1\right). \tag{62}$$

In addition, we also need the equation for $\sin\beta$, which is given by (using a right triangle)

$$\sin\beta = \frac{1}{e}\sqrt{e^2 - \left[\frac{a(1-e^2)}{r} - 1\right]^2}, \tag{63}$$

so that $\tan\beta$ is

$$\tan\beta = \frac{\sqrt{e^2 - \left[\frac{a(1-e^2)}{r} - 1\right]^2}}{\frac{a(1-e^2)}{r} - 1}. \tag{64}$$

We found that the distance the secondary ejecta travels is given by the arc length of Moon the orbit travels greater than the radius of the Moon:

$$D = 2(\pi - \beta)r_m, \tag{65}$$

or solving for the angle β,

$$\beta = \pi - \frac{D}{2r_m}. \tag{66}$$

[3]See Eqs. 4.30 and 4.32 from http://www.braeunig.us/space/orbmech.htm.

Using Eqs. 59 and 60, we can write

$$\frac{a}{r_m}(1-e^2) = 2\frac{v^2}{v_{esc}^2}\sin^2\gamma, \tag{67}$$

so Eq. 64 becomes [c.f., Eq. (1) of *Vickery*, 1986]

$$\tan\left(\frac{D}{2r_m}\right) = \frac{2\frac{v^2}{v_{esc}^2}\sin\gamma\cos\gamma}{1-2\frac{v^2}{v_{esc}^2}\sin^2\gamma} = \frac{\frac{v^2}{v_{esc}^2}\sin(2\gamma)}{\frac{v^2}{v_{esc}^2}[\cos(2\gamma)-1]+1} = \frac{2\frac{v^2}{v_{esc}^2}\tan\gamma}{1+(1-2\frac{v^2}{v_{esc}^2})\tan^2\gamma}. \tag{68}$$

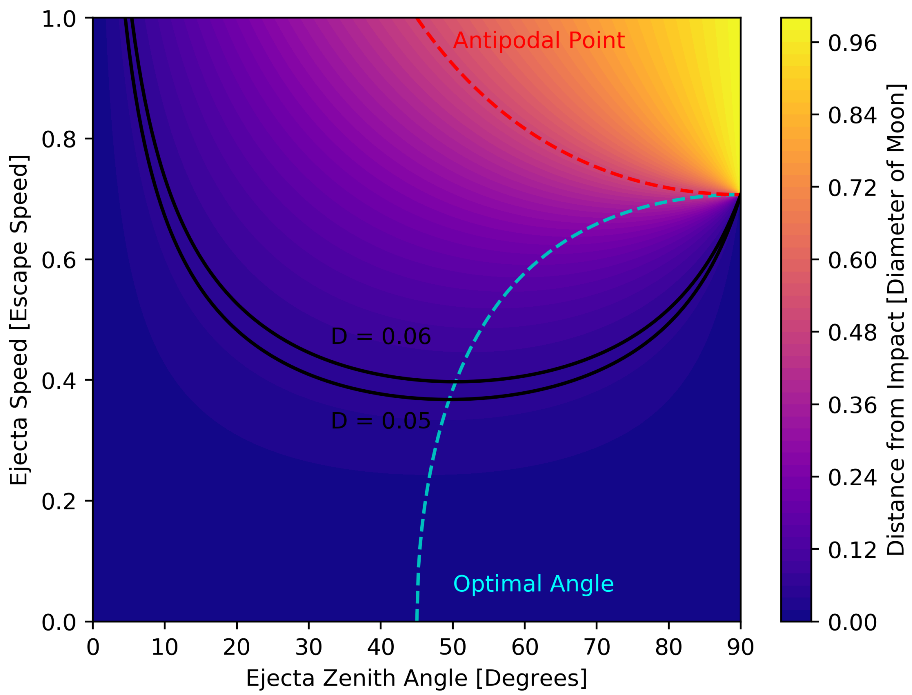

Figure 4: The color gradient shows the distance a projectile goes with a given ejected speed and zenith angle. The cyan dashed line gives the optimal angle for a given speed to reach the furthest distance, i.e., Eq. (74). The red dashed line shows for which pairs of speeds and zenith angles are required to hit the antipodal point. As an example, all ejecta with speed and angle pairs between the two black curves will reach a location between 0.05 and 0.06 lunar circumference units away, using Eq. (71).

For $D \ll 2r_m$, the optimum angle that gives the smallest velocity needed is $45°$. In other words, for a given velocity, the greatest distance is found by taking $\gamma = 45°$. However, if the distance D is roughly the same order as the diameter of the Moon

$2r_m$, ($D > 0.01 \times 2r_m$), then the optimal angle from zenith is greater than $45°$, i.e. a shallower angle to the horizon. This is because at large velocities, the curvature of the Moon comes into play. For larger velocities, there are also angles γ that cannot reach a distance D. Allowable angles (in radians) that can travel a distance D are defined by

$$\gamma > \frac{D}{4r_m}. \tag{69}$$

In other words, the maximum distance the ejecta can reach for a given angle is

$$D = 4\gamma r_m. \tag{70}$$

For example, from this equation we can conclude that for $\gamma < 45°$, the ejecta will not reach the antipodal point, see Figure 4.

Solving for v we have

$$\frac{v}{v_{esc}} = \frac{+1}{\sqrt{\sin(2\gamma)\left(\cot\left(\frac{D}{2r_m}\right) + \tan\gamma\right)}} = \frac{+1}{\sqrt{1 + \sin(2\gamma)\cot\left(\frac{D}{2r_m}\right) - \cos(2\gamma)}}. \tag{71}$$

We can also solve for the zenith angle γ, given by

$$\cot\gamma = x^2 \cot\left(\frac{D}{2r_m}\right) \pm \sqrt{x^4 \cot^2\left(\frac{D}{2r_m}\right) + (2x^2 - 1)}, \tag{72}$$

where $x = v/v_{esc}$. Solving for the discriminant, the minimum x can be for a given distance D is

$$x_{min}^2 = \tan^2\left(\frac{D}{2r_m}\right)\left[\csc\left(\frac{D}{2r_m}\right) - 1\right]. \tag{73}$$

Plugging into Equation 72, the optimal angle from zenith is given by

$$\cot\gamma_{opt} = \sec\left(\frac{D}{2r_m}\right) - \tan\left(\frac{D}{2r_m}\right). \tag{74}$$

In terms of x, we have

$$\cos(2\gamma_{opt}) = \frac{x^2}{x^2 - 1}. \tag{75}$$

Once $D > \pi r_m$, the optimal angle is $\gamma = 90°$, i.e., parallel to the horizon. For small distances $D \ll 2r_m$, the optimal angle is $\gamma = 45°$, as mentioned above.

5.7 Distance and Bearing

Given two latitude-longitude points on a sphere, (ϕ_1, θ_1) and (ϕ_2, θ_2), we can compute the distance and bearing following Chris Veness's webpage[4].

[4] https://www.movable-type.co.uk/scripts/latlong.html

The distance D is given by the equation

$$\tan\left(\frac{D}{2r_m}\right) = \sqrt{\frac{a}{1-a}}, \tag{76}$$

where a is given by

$$a = \sin^2(\Delta\phi/2) + \cos\phi_1\cos\phi_2\sin^2(\Delta\lambda/2), \tag{77}$$

for $\Delta\phi = \phi_2 - \phi 1$ and $\Delta\lambda = \lambda_2 - \lambda_1$. Solving for the distance and simplifying, we have

$$D = 2r_m \arcsin(\sqrt{a}), \tag{78}$$

or

$$D = 2r_m \arccos(\sqrt{1-a}). \tag{79}$$

Other useful expressions involving trigonometric functions of D/r_m are

$$\sin(D/r_m) = 2\sqrt{a(1-a)}, \tag{80}$$
$$\cos(D/r_m) = 1 - 2a, \tag{81}$$
$$\tan(D/r_m) = \frac{2\sqrt{a(1-a)}}{1-2a}. \tag{82}$$

Eq. (76) is the shortest distance between two coordinate points. For the long-distance, use

$$\tan\left(\pi - \frac{D}{2r_m}\right) = -\tan\left(\frac{D}{2r_m}\right) = \sqrt{\frac{a}{1-a}}. \tag{83}$$

The initial bearing θ (from due East) is given by the following equation (assuming the short-distance):

$$\tan\theta_{i(1,2)} = \frac{\sin\Delta\lambda\cos\phi_2}{\cos\phi_1\sin\phi_2 - \sin\phi_1\cos\phi_2\cos\Delta\lambda}. \tag{84}$$

To find the final bearing (assuming the short-distance), swap $\phi_1 \longleftrightarrow \phi_2$ and $\lambda_1 \longleftrightarrow \lambda_2$ and reverse the angle such that

$$\theta_{f(1,2)} = (\theta_{i(2,1)} + \pi) \mod 2\pi. \tag{85}$$

In order to compute the initial and final bearing for the long-distance trajectory, add π and then mod by 2π to Eqs. (84) and (85). In other words, swap initial and final bearings $\theta_{i(1,2)} \longleftrightarrow \theta_{f(1,2)}$.

We can also get the final latitude and longitude if we are given the distance D and bearing θ from the starting location. The latitude and longitude are given by

$$\phi_2 = \arcsin\left[\sin\phi_1\cos(D/r_m) + \cos\phi_1\sin(D/r_m)\cos\theta\right], \tag{86}$$
$$\lambda_2 = \lambda_1 + \arctan\left[\frac{\sin\theta\sin(D/r_m)\cos\phi_1}{\cos(D/r_m) - \sin\phi_1\sin\phi_2}\right]. \tag{87}$$

References

Carrier III, W. D., Particle size distribution of lunar soil, *Journal of Geotechnical and Geoenvironmental Engineering*, *129*(10), 956–959, 2003.

Gault, D. E., and J. A. Wedekind, Experimental studies of oblique impact, in *Lunar and Planetary Science Conference Proceedings*, vol. 9, pp. 3843–3875, 1978.

Housen, K. R., and K. A. Holsapple, Ejecta from impact craters, *Icarus*, *211*(1), 856–875, 2011.

Miller, A., Esabase2 debris release 10.0 technical description, *Tech. Rep. 1.7*, ESA, 2017.

Rival, M., and J. Mandeville, Modeling of ejecta produced upon hypervelocity impacts, *Space debris*, *1*(1), 45–57, 1999.

Shuvalov, V., Ejecta deposition after oblique impacts: An influence of impact scale, *Meteoritics & Planetary Science*, *46*(11), 1713–1718, 2011.

Vickery, A., Size-velocity distribution of large ejecta fragments, *Icarus*, *67*(2), 224–236, 1986.